DOI: 10.24352/UB.OVGU-2017-117 TECHNISCHE MECHANIK, 37, 2-5, (2017), 409-421
submitted: April 06, 2017

Turbocharger Dynamic Analysis: Advanced Design Simulation in Time Domain Using CFD Predicted Thermal Boundary Conditions

S. Bukovnik, G. Offner, A. Diemath, L. Smolik

Small changes of surface temperature, clearance and bearing profile can significantly change stiffness and damping characteristics of slider bearings. This may influence dynamics and in case of turbochargers the rotor radial deflection. Noise, Vibration, Harshness (NVH) or durability issues like rotor colliding with housing may be implied as a consequence.
This paper presents a new methodology for dynamic turbocharger investigation. It considers multi-body dynamics (MBD) of flexible rotor and housing structures coupled with elasto-hydrodynamics (EHD) of the inner and outer oil film. The energy equation for calculation of oil film temperature is considered in EHD using thermal boundary condition obtained from 3D computational fluid dynamics (CFD) simulation. Typical targets for CFD simulation within the turbocharger development process are flow and thermal investigation as well as specifically providing accurate thermal boundary condition for thermo-mechanical fatigue analysis. For this purpose CFD analysis considers a fully coupled fluid-structure interaction. However, the same CFD model can be used to provide the required boundary conditions for dynamic analysis as well. The bearing profiles under thermal load are derived from Finite Element (FEM) analysis based on same thermal boundary conditions.
The authors demonstrate the application of the methodology for a typical turbocharger design study applied for heavy-duty engines with full floating bushings that have radial bore connections between inner and outer oil films. The rotor operating speed reaches up to 110 krpm. Dynamic simulation results with nominal clearance and temperature are compared with the results obtained when CFD and FEM predicted boundary conditions are used. Based on results for the oil film pressure and flow through each oil film as well as flow between inner and outer oil film a valid conclusion about the rotor dynamic behaviour, bearing mechanical and thermal loads can be made. The presented methodology proves to be a next level approach in prediction of turbocharger simulation in the development process.

1 Introduction

In recent years the number of turbo charged combustion engines has dramatically increased. Turbocharger manufacturers are required to provide the optimized designs of turbochargers for a variety of combustion engines, which means a large effort for design optimization and testing is necessary. Simulation tools can be used to speed up the design and optimization process and reduce its cost and time. There are existing simulation approaches which can be used for the detailed dynamic analysis of the turbocharger behaviour. Such refined simulation approaches consider effects of rotor flexibility, unbalance distribution, gyroscopic effects, interaction of the oil films and structure and even coupling of inner and outer oil film for the full floating bushings design. However, to obtain accurate results a detailed information about the oil property in the bearings, especially the oil viscosity is needed. Oil viscosity is typically assumed as constant which is based on the assumed temperature. Alternatively measured oil temperature can be used for determination of oil viscosity. When temperature is measured this is typically done at the location where oil enters the turbocharger housing and not in the oil film. As turbochargers can operate at very high temperatures, the heat that spreads from the turbine side through the structure to the oil film might influence the temperature of the oil. In addition, due to the rotation of the rotor and floating bushing, heat is generated in the oil film due to viscos friction. This heat is dissipated to the surrounding structure but it also heats up the oil film. AVL EXCITE^{TM} offers the possibility to consider the energy equation of the oil film in combination with its elasto-hydrodynamics. With this approach it is possible to consider the correct temperature distribution within the oil film and by this a correct oil viscosity over time.
Boundary condition for the oil film energy equation is structure temperature. This temperature is not uniform. It is strongly influenced by the heat coming from the turbine side and by cooling effects of the cold air at the compressor side. A typical temperature distribution in the turbocharger housing is shown in Figure 1.

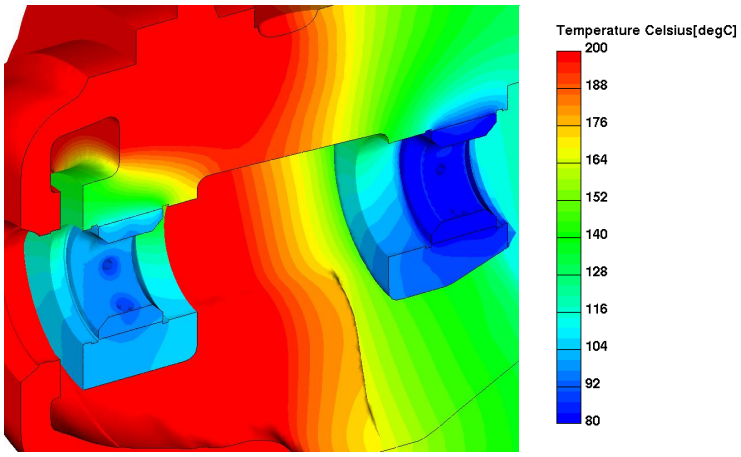

Figure 1. Typical temperature distribution in turbocharger housing

The consideration of the structure temperature distribution, is also done based on results of preliminary CFD calculation. Interacting surfaces of the turbocharger housing and floating bushing as well as floating bushing and the rotor are typically assumed as perfect cylinders in dynamic simulation. Under high temperature load, especially at the turbine side, thermal deformation of the structure is not uniform due to the unsymmetrical geometry of the turbocharger housing as well as the unsymmetrical temperature distribution in the housing structure. The deviation of the shape from the perfect cylinder at bearing surfaces can be several microns which is already a relevant percentage of the clearance and which therefore must not be neglected in order to be able to predict accurate oil film pressure distributions. This deviation can be considered in the dynamic simulation model as deviations of the cylindrical shape in radial direction, which can be defined as a surface map. Such maps can be obtained as a result of thermal structure analysis performed using FEM. The thermal boundary conditions for the FEM calculations are structure temperatures which again are obtained from CFD calculation.

2 Turbocharger used for this Investigation

The turbocharger used to demonstrate the methodology in this paper is the existing design applied for heavy-duty engines with full floating bushings that have 6 radial bore connections that connect outer and inner oil films. The rotor is axially supported with axial bearings close to the compressor wheel. Axial motion of the floating bushings is supported by the two circlips per floating bushing that are mounted in the housing.
The housing of the turbocharger is made of steel. The compressor wheel is made of aluminium and the rotor shaft and the turbine wheel are made of steel as well. The total rotor mass is about 1 kg of which the compressor wheel is about 0.19 kg and the turbine wheel is 0.56 kg. Unbalance is applied at both wheels, at wheel nose and wheel back separately. The level of unbalance is 0.6 to 0.8 gmm at the wheel nose and 0.9 to 1.3 gmm at the wheel back. The rotor operating speed reaches up to 110 krpm. The oil used in this turbocharger is SAE 10W-40. It is supplied in both outer oil films via a bore in the housing. The oil supply pressure is 3 bar, while the assumed temperature of the supplied oil is 90 degC.

3 CFD Simulation Model

This section briefly describes the fluid dynamics and conjugate heat transfer as part of the general multi-physics approach, which is implemented in the commercial CFD code AVL FIRE^{TM}, Basara et al. (2009) and AVL List (2017). In this multi-material approach, temperatures and local heat transfer coefficients on domain interfaces are exchanged after each iteration step considering implicitly coupled fluid and structure domains. Hence, the temperature distribution within the structural part of the turbocharger is also obtained from the steady CFD simulation. The steady CFD simulation for the highest exhaust gas temperature and exhaust gas flow is selected in order to obtain the highest possible structure temperature and by this the worst conditions for the oil films. The methodology is based on the fully conservative finite-volume method adopted for unstructured meshes which can contain computational cells of any shape. All dependent variables, such as momentum, pressure, density, turbulence kinetic energy, dissipation rate, and total enthalpy / temperature are calculated at the cell center. For fluid parts, such as gas flow in the turbine and compressor domains, the Reynolds-Averaged Navier-Stokes

(RANS) equations are used for numerical simulations. The rotational motion of the compressor and the turbine is modelled via the method of moving reference frame (MRF), Luo et al. (1994). The simulation mesh, which is used for the multi-material simulation, counts in total 7.17 million polyhedral cells. The entire mesh consists of 15 domains, whereas 13 domains are solid materials of various material properties, as shown in Figure 2, and the remaining two domains contain the calculated gas flow for exhaust gas residual (EGR) from the turbine side and air from the compressor side.

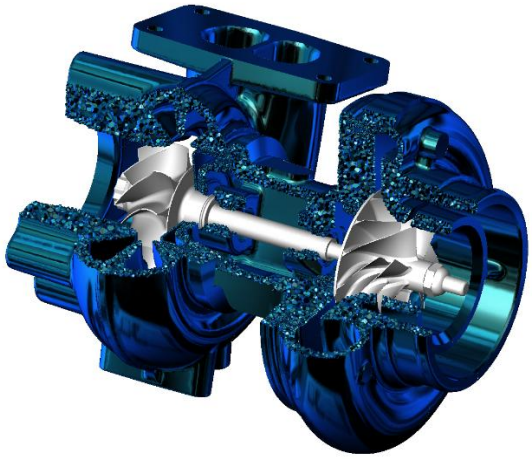

Figure 2. Structural parts of multi-material simulation model.

Figure 3 left displays the temperature field for the entire structural part gathered for the exemplary operating point at 80.7 krpm rotor speed. The corresponding temperature in an axial cross section of the flow field and structural part in the turbine section is shown in the right picture of Figure 3.

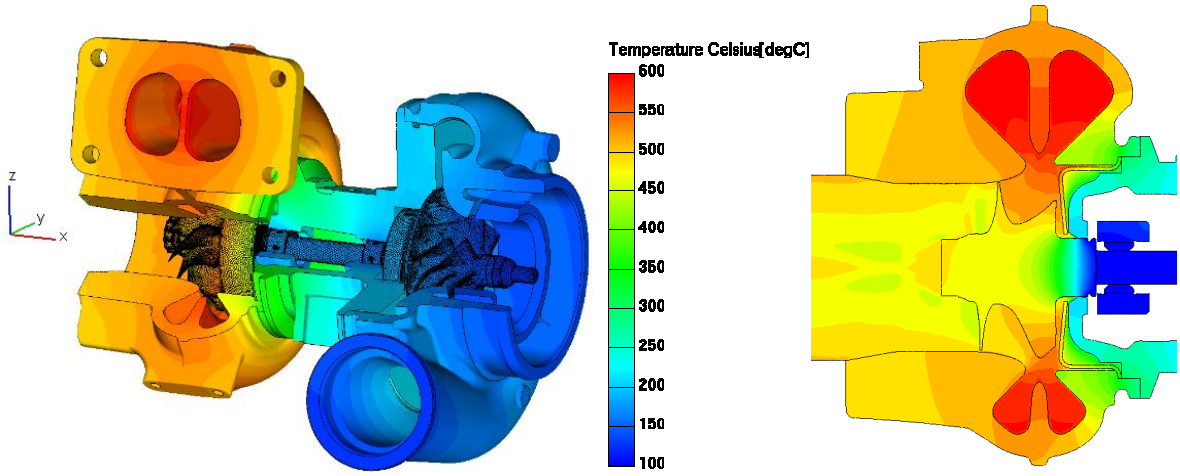

Figure 3. Temperature distribution in entire structure (left) and in a fluid/structure turbine cross section (right).

CFD simulations are typically done for a flow and thermal investigation as well as for providing accurate thermal boundary condition for thermo-mechanical fatigue analysis. In the investigation shown in this paper the condition with the hottest structure observed during CFD analysis is used as a boundary condition for the dynamics investigation. Structure deformed shape under the thermal load obtained from CFD is computed using FEM as shown in Figure 4. The FEM results in the figure are enlarged by a factor of 300.

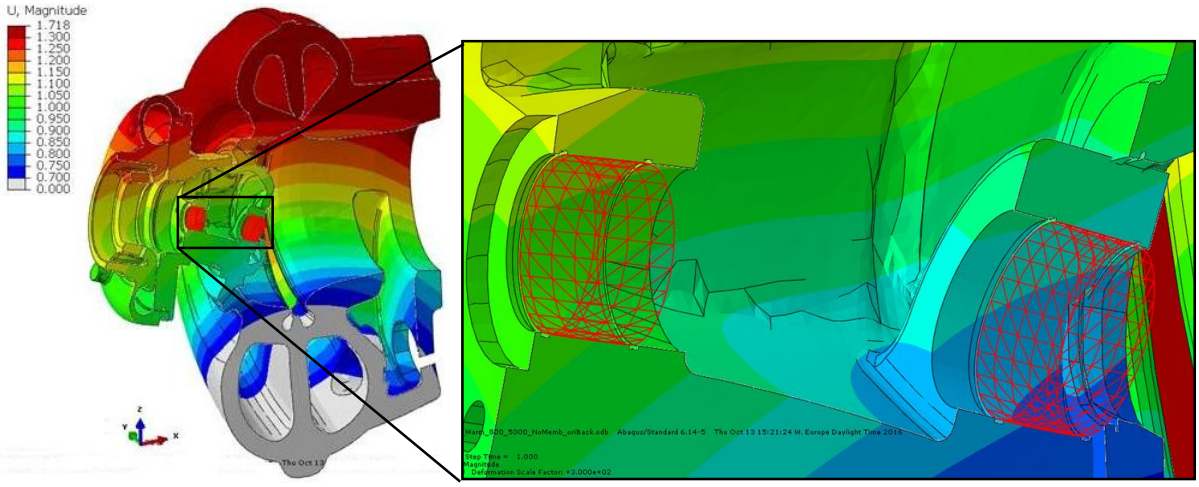

Figure 4. Turbocharger housing (left) and zoomed into the area of bearings (right) under thermal deformation.

4 Dynamic Simulation Model

Figure 5 shows a schematic representation of the turbocharger simulation model, which is used in this paper. The major components, which need to be considered, are housing and rotor that are considered as flexible bodies, which itself is supported by two bearings. Each bearing consists of an inner and an outer oil film and a floating bushing that is also a flexible body. Inner and outer oil films are connected via six drillings in the bushing, respectively. The according mathematical sub-models will be briefly introduced in the following sections. For more details of the sub-models as well as their coupling, refer to Offner (2013). During simulation, the coupled sub-models are solved in time domain using numerical time integration.

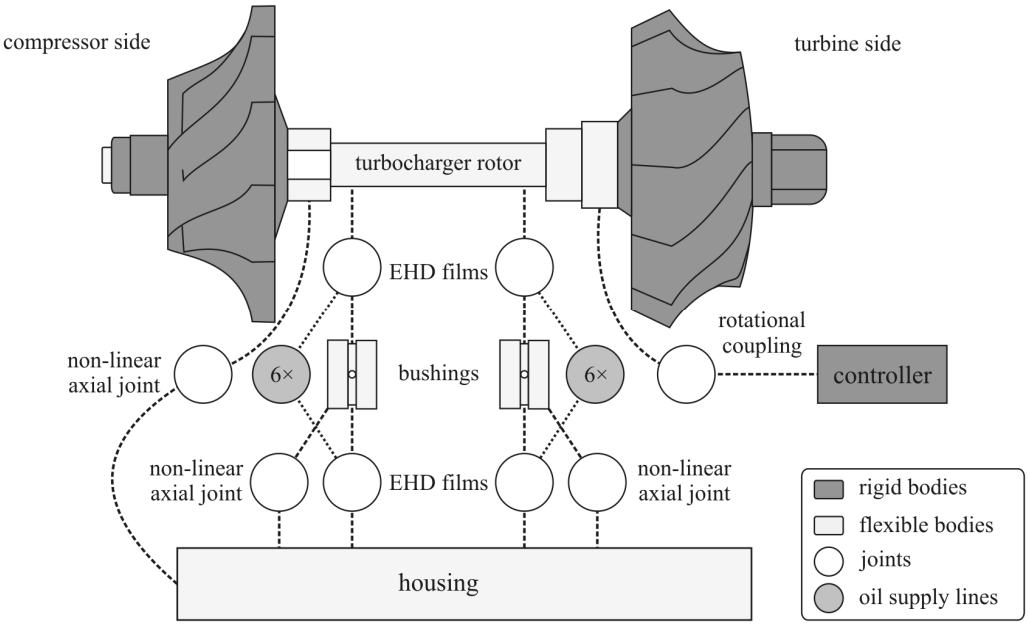

Figure 5. Schematic representation of the AVL EXCITE ^{TM} simulation model of the investigated turbocharger

Structural Components

Each structural component is represented by a body, which is modelled according to the floating frame of reference formulation (FFoR), see Offner (2011) for details. The formulation allows to distinguish global motion and local elastic deformation. Accordingly, the equations of motion for a structured flexible body, Parikyan et al. (2001), read

$$\begin{aligned} \boldsymbol{M}\cdot\ddot{\boldsymbol{q}}+\boldsymbol{D}\cdot\dot{\boldsymbol{q}}+\boldsymbol{K}\cdot\boldsymbol{q} &= \boldsymbol{f}^{*}+\boldsymbol{f}^{a}+\boldsymbol{f}^{gyros}-\boldsymbol{f}^{rbAcc} \\ \boldsymbol{S}(\boldsymbol{\theta}_B)\cdot\dot{\boldsymbol{\theta}}_B &= \boldsymbol{\omega} \\ \boldsymbol{\theta}_B^T\cdot\boldsymbol{\theta}_B &= 1 \\ \boldsymbol{r}(\boldsymbol{q}) &= \boldsymbol{0} \end{aligned} \quad . \tag{1}$$

This differential algebraic equation system describes the global motion and local vibrational behaviour of a flexible body and is solved with respect to the vector of unknowns, which reads

$$\boldsymbol{z}=\left(\boldsymbol{x}_B{}^T,\boldsymbol{\theta}_B{}^T,\dot{\boldsymbol{x}}_B{}^T,\boldsymbol{\omega}^T,\boldsymbol{q}^T,\dot{\boldsymbol{q}}^T\right)^T \tag{2}$$

and which considers the global position and orientation coordinates ($\boldsymbol{x}_B\in\Re^3$ and $\boldsymbol{\theta}_B\in\Re^4$), the velocity vectors $\boldsymbol{\omega}\in\Re^3$ and $\dot{\boldsymbol{x}}_B\in\Re^3$ as well as the generalized displacement vector $\boldsymbol{q}$ and its first time derivative. $\boldsymbol{q}$ represents the elastic deformations of the total body, considering a space discretization with N nodes

$$\boldsymbol{q}=\left(\boldsymbol{q}_1^T,\boldsymbol{q}_2^T,...,\boldsymbol{q}_N^T\right)^T . \tag{3}$$

The vector of local displacements $\boldsymbol{q}_i$ of any node i consists of

$$\boldsymbol{q}_i=\begin{pmatrix}\boldsymbol{u}_i\\ \boldsymbol{\varphi}_i\end{pmatrix}=\left(u_{i,1},u_{i,2},u_{i,3},\varphi_{i,1},\varphi_{i,2},\varphi_{i,3}\right)^T , \tag{4}$$

with the translatorial displacement components $u_{i,1}$, $u_{i,2}$ and $u_{i,3}$ and the rotational displacement components $\varphi_{i,1}$, $\varphi_{i,2}$ and $\varphi_{i,3}$.

The matrices $\boldsymbol{M}$, $\boldsymbol{D}$ and $\boldsymbol{K}$ are the time invariant mass, damping and stiffness matrix, which can be generated in a pre-processing step using commercial FEM software. The right-hand side of the ordinary differential equation sums up acting body forces. It contains inertia, external and joint forces. The inertia forces $\boldsymbol{f}^{gyros}$ and $\boldsymbol{f}^{rbAcc}$ result from the global motion of the body and denote the rigid body acceleration forces and the gyroscopic forces, respectively. External forces like axial or radial forces at the compressor or turbine wheel are considered in the vector $\boldsymbol{f}^{a}$. Those forces are given functions over time and can, for instance, be obtained by preceding measurement or pre-calculation. Forces, which occur due to contact to other component surfaces as for instance those in radial slider bearings, are considered in $\boldsymbol{f}^{*}$.

$\boldsymbol{\theta}_B$ are quaternions representing the orientation of the body coordinate system with respect to the inertial coordinate system. The quaternion normalization condition $\boldsymbol{\theta}_B^T\cdot\boldsymbol{\theta}_B=1$ must hold. The matrix $\boldsymbol{S}(\boldsymbol{\theta}_B)$ is used to transform the time derivative of the Euler parameters into the vector of the body's global angular velocities $\boldsymbol{\omega}$. For distinguishing gross and local motions, a reference condition is given by the last equation $\boldsymbol{r}(\boldsymbol{q})=\boldsymbol{0}$, which considers

$$\boldsymbol{r}(\boldsymbol{q})=\begin{pmatrix}\boldsymbol{r}_1(\boldsymbol{q})\\ \boldsymbol{r}_2(\boldsymbol{q})\end{pmatrix}=\begin{pmatrix}\sum_{i=1}^{N}m_i\cdot\boldsymbol{u}_i\\ \sum_{i=1}^{N}m_i\cdot\boldsymbol{A}_{c_i}\cdot\boldsymbol{u}_i+\boldsymbol{I}_i\cdot\boldsymbol{\varphi}_i\end{pmatrix}. \tag{5}$$

$\boldsymbol{A}_{c_i}$ is a skew symmetric matrix operator, which is applied to the position vector $\boldsymbol{c}_i$ of node i, reading

$$\boldsymbol{A}_{c_i}=\begin{pmatrix}0 & -c_{i,3} & c_{i,2}\\ c_{i,3} & 0 & -c_{i,1}\\ -c_{i,2} & c_{i,1} & 0\end{pmatrix}. \tag{6}$$

m_i and $\boldsymbol{I}_i$ denote mass and tensor of inertia of any node i. Equation (5) is motivated by the assumption that local deformation have to remain as small as possible which assures the validity of the linearization used for linear elasticity theory.
Equation (1) is used in case of rotor but also in case of both floating bushings. As the housing body performs no global motion, equation (1) reduces to the dynamic ordinary differential equation in this case. For further details on the differential algebraic equation but also its solution algorithms refer to Drab et al. (2009).

Oil Film in Radial Slider Bearings

The hydrodynamic contacts are represented by an averaged Reynolds equation, which, formulated with respect to the outer sliding body coordinate system, reads

$$-\frac{\partial}{\partial x}\left(\frac{\theta\cdot\varphi_x\cdot h^3}{12\eta}\frac{\partial p}{\partial x}\right)-\frac{\partial}{\partial z}\left(\frac{\theta\cdot\varphi_z\cdot h^3}{12\eta}\frac{\partial p}{\partial z}\right)+\frac{u_i-u_o}{2}\frac{\partial\left(\left(\tilde{h}_T+\sigma\cdot\varphi_s\right)\cdot\theta\right)}{\partial\bar{x}}+\frac{\partial\left(\tilde{h}_T\cdot\theta\right)}{\partial t}=0 \quad (7)$$

$h=h\,(x,z,t)$ represents the nominal clearance gap height between the two sliding surfaces. h is measured in y coordinates and considers the deformed shape of the structure under the thermal load, see Figure 4. x, y and z are the circumferential, the radial and the axial direction of the bearing. θ is the fill ratio, so the percentage of h, which is filled with oil. The surfaces slide with a velocity of u_i and u_o in x direction. i and o denote the surface of the inner and outer sliding body, respectively. These are the journal and the bushing surface in case of the inner oil film and the bushing and the housing in case of the outer oil film. η is the dynamic viscosity of the lubricant, which may depend on the lubricant's temperature T. The oil film temperature distribution of the lubricant is calculated by an averaged formulation of the energy equation. Bearing shell and journal structure temperatures are based on the three-dimensional heat conduction equation. Pre-calculated temperature boundary conditions (Figure 3) are considered at the surface of the inner and at the outer sliding body. See Lorenz (2015) for further details.
Equation (7) considers flow factors φ_x, φ_z and φ_s obtained according to Patir and Cheng (1978), assuming Gaussian distributed surface heights. σ is a composite roughness value, which can be computed from the standard deviation of the clearance height of the two sliding surfaces σ_i and σ_o via $\sigma=\sqrt{\sigma_i^2+\sigma_o^2}$. The local oil film thickness h_T considers random roughness amplitudes with respect to the mean shape of the surfaces, respectively, where $h_T=h+\delta_i+\delta_o$ and $\tilde{h}_T$ is the local mean value of h_T assuming Gaussian distribution.
Equation (7) is solved with respect to the hydrodynamic pressure p in lubricated areas and with respect to the oil vapour fraction θ in cavitation areas. Bushing drillings and therefore couplings between inner and outer oil film are considered in terms of boundary conditions. The pressure in the boundary condition is obtained employing oil supply line model in each drilling, Offner et al. (2013). In each drilling the oil is assumed to be incompressible with isothermal viscosity. The flow in each drilling is described by a steady state 1D Euler equation, i.e. Bernoulli equation. Fictitious force effects, which result from the motion of the bushing, and cavitation effects in the line are also considered.
In order to consider physical metal to metal contact, a local asperity pressure is computed in dry and mixed lubricated contact areas. The model developed by Greenwood and Tripp (1970-1971), is applied for that purpose.

5 Dynamic Results

Simulations are performed for constant speeds from 10 krpm up to 110 krpm every 10 krpm. Alternatively, rotor run-up for the same speed range is possible as a single calculation. Constant rotor speeds approach is selected due to available processors so that all speeds could run in parallel and the results are available in the shorter time. During the transient simulation viscos friction in oil films acts on rotor and floating bushings and influence their rotational speed. The speed of the floating bushings changes depending on the balance of the friction forces from the inner and the outer oil film. An initial speed of the rotor and floating bushings needs to be defined in terms of initial conditions. As these structural initial conditions typically are inaccurate, a number of rotor rotations are

required until the rotational speed of the floating bushings becomes stable. Therefore, the calculations are performed for up to 360 rotor rotations to ensure stable floating bushing speeds.
In the case of a turbocharger rotor that rotates at high speeds the dominant forces are implied by unbalances of the rotor wheels.
For each speed case two dynamic calculations are performed, the first one considers a perfect cylindrical shape of the bore, with nominal hot clearance and considering constant oil viscosity based on the assumed oil film temperature. This case is in further text referenced as nominal case. The second case considers a deformed housing shape (FEM) under thermal load and with CFD pre-calculated surface temperatures of the housing, rotor and floating bushings. In the second case viscosity is changing depending on the oil film temperature that is determined by solving energy equation for the oil film. An example of floating bushing temperatures that are used as boundary conditions are shown in the Figure 7.

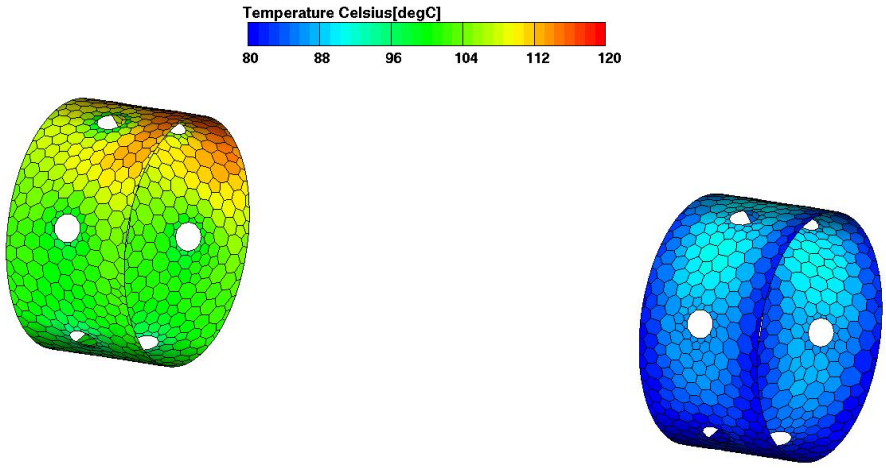

Figure 7. Floating bushing temperature used as boundary conditions for energy equation of the outer oil film

Oil Temperature

Oil film temperatures over speed are depicted in Figure 8. An assumed constant temperature of 90 degC for each oil film is shown in the same diagram with calculated temperatures, maximum and minimum that appear in the oil film for the dynamic simulation using CFD pre-calculated temperature distribution. During the simulation with consideration of energy equation in the oil film, the hydrodynamic friction in the oil film heats up the oil. Depending on the temperature difference of the oil film and the surrounding structure the heat is transferred from the oil to the structure or vice versa. It can be seen that oil film temperatures differ significantly from the assumptions made in the nominal case. In the outer oil film at the compressor side the assumption is relatively good as the obtained temperatures are ranging between 85 and 95 degC. At the outer film at turbine side temperatures are in a range of 105 to 115 degC. This is mainly due to the hotter housing structure that heats up the oil in the film. For the inner oil film the temperatures are much higher than assumed especially at the higher speed due to the oil heat up from the viscous friction. The results demonstrate that it is not possible to assume an accurate constant temperature that could be applied for the complete speed range of the turbocharger.

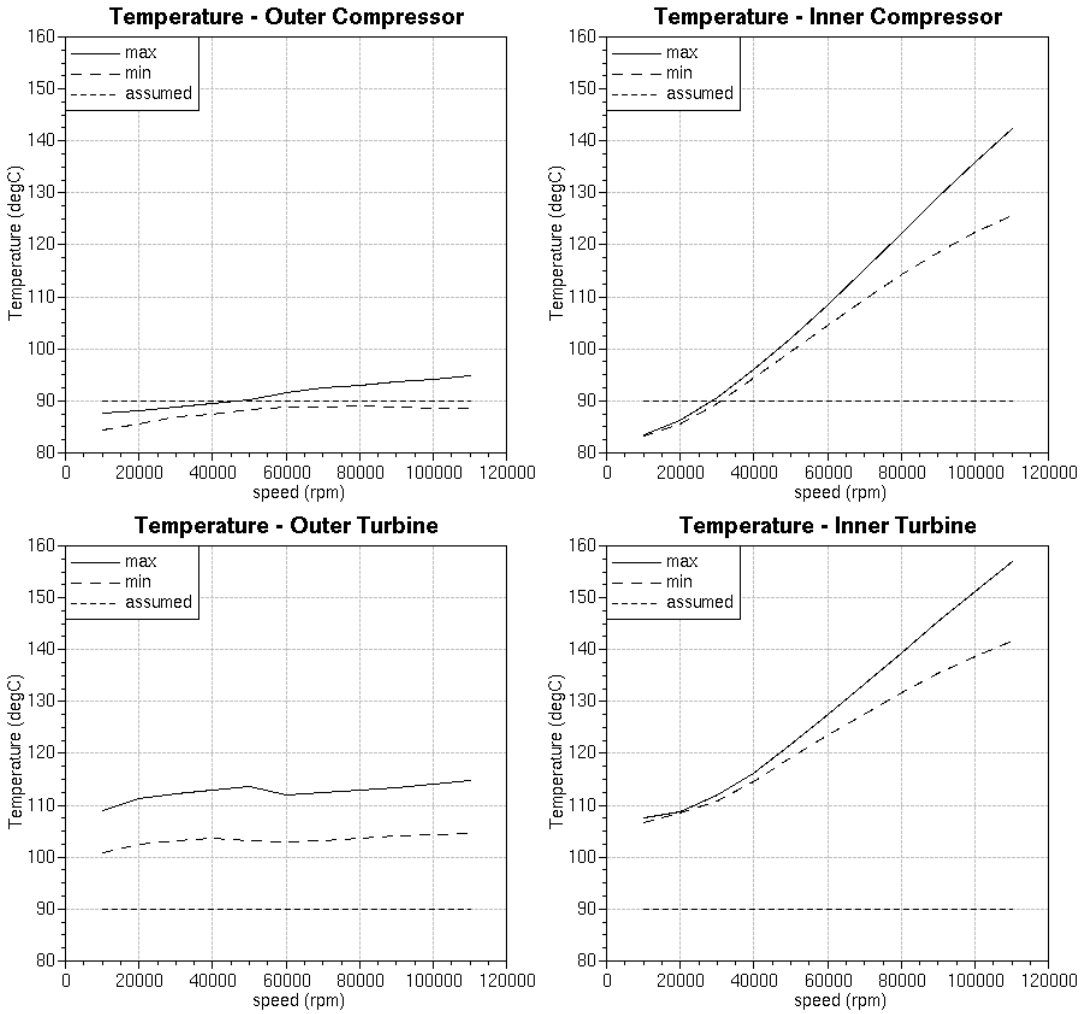

Figure 8. Oil film temperatures over speed: assumed constant temperature versus calculated minimum and maximum temperature using CFD and FEM pre-calculated boundary conditions

Oil Viscosity

Oil viscosity changes during the rotor operation depending mainly on temperature. The dependence on pressure and shear rate is assumed to be negligible in the present study. Results for maximum and minimum oil viscosity in each oil film over speed are shown in the Figure 9. It can be seen that at the compressor side outer film viscosity is relatively similar to the assumed value. For the inner film at the compressor side it is similar only for the lower speeds range. At the turbine side the assumed viscosity is significantly higher than the real one obtained in the simulation, which follows the previous conclusion that assumed temperature is too low at the turbine side.

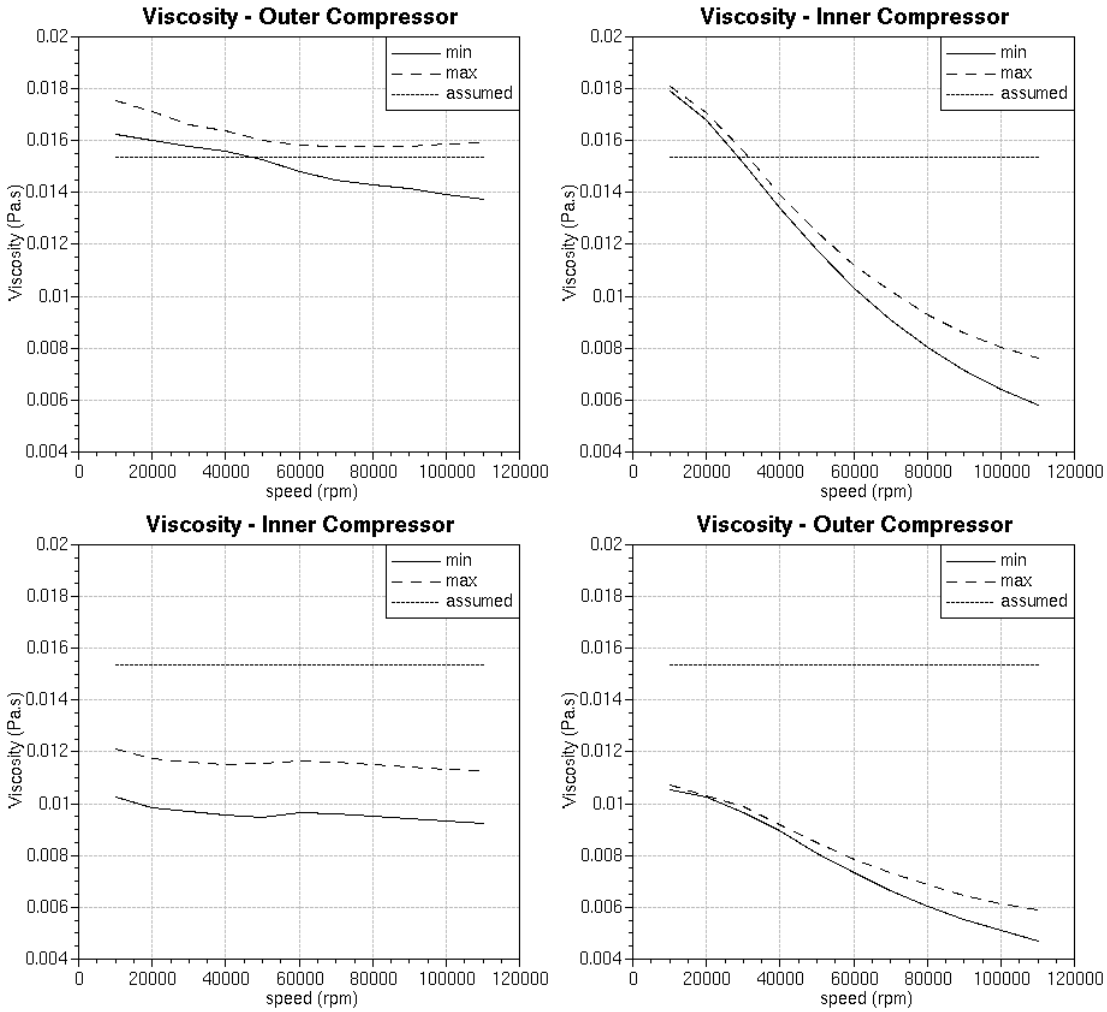

Figure 9. Dynamic viscosity in oil films over speed: constant viscosity (assumed) versus calculated minimum and maximum viscosity using CFD and FEM pre-calculates boundary conditions

Speeds of the Floating Bushings

Floating bushing rotational speeds are a further result of the dynamic simulation. Floating bushings rotate under the influence of viscous friction in oil film. Pressure, fill ratio and temperature and by this also viscosity in the oil films dynamically changes. This implies changing friction load on the floating bushing which leads to dynamically changing floating bushing speeds. Nevertheless, the mean speed of the floating bushing stabilizes after a few seconds. The mean floating bushing speeds over the rotor speeds are shown for both simulation cases in Figure 10. Solid line curves show the results for the nominal case with assumed temperature while the dashed line curves show the results for the CFD and FEM pre-calculated boundary conditions. The speed of the floating bushings are very similar in the lower rotor speed range and differ significantly in the higher speed range for the case with CFD and FEM pre-calculated boundary conditions. This is mainly influenced by lower viscosity in the inner oil films. Another influence is the lower clearance at outer oil films due to the higher temperature at the turbine side. The material of the floating bushing has higher thermal expansion compared to the housing. This means the floating bushing expands more and by this reduces the outer oil film clearance.

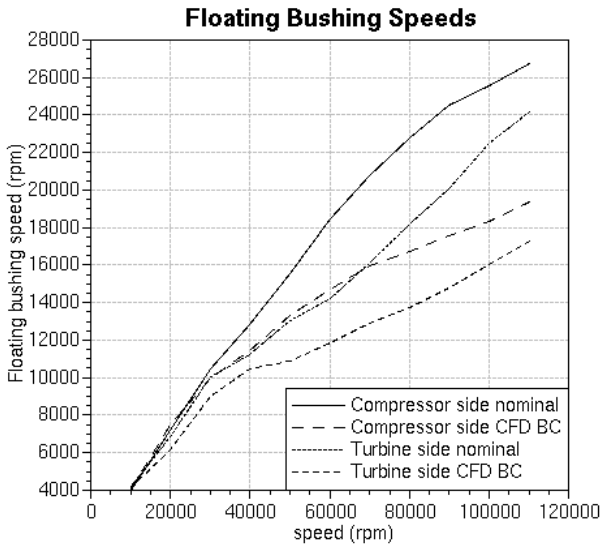

Figure 10. Rotational speed of floating bushings at compressor and turbine for nominal case with assumed temperature versus case with CFD and FEM pre- calculated temperature

Displacement at the Compressor Nut

Typical results, which also can be measured, are displacements of the rotor nut. The result for the maximum and minimum displacement in vertical direction Z with respect to the housing coordinate system and the frequency content of this displacement is shown in Figure 11 for nominal simulation and in Figure 12 for the simulation that uses CFD and FEM pre-calculated boundary conditions. In both cases significant vibrations are of lower sub-harmonic while the first order vibrations are only slightly visible. There is a strong difference between the cases with nominal and pre-calculated boundary conditions. The amplitude of motion is significantly smaller in case of using CFD and FEM pre-calculated boundary conditions. This is influenced mainly by lower clearance at the outer bearing especially at the turbine side. At higher temperature, floating bushings will have higher expansion due to the material with higher expansion coefficient compared to the housing material which will result in smaller clearance at outer oil films.

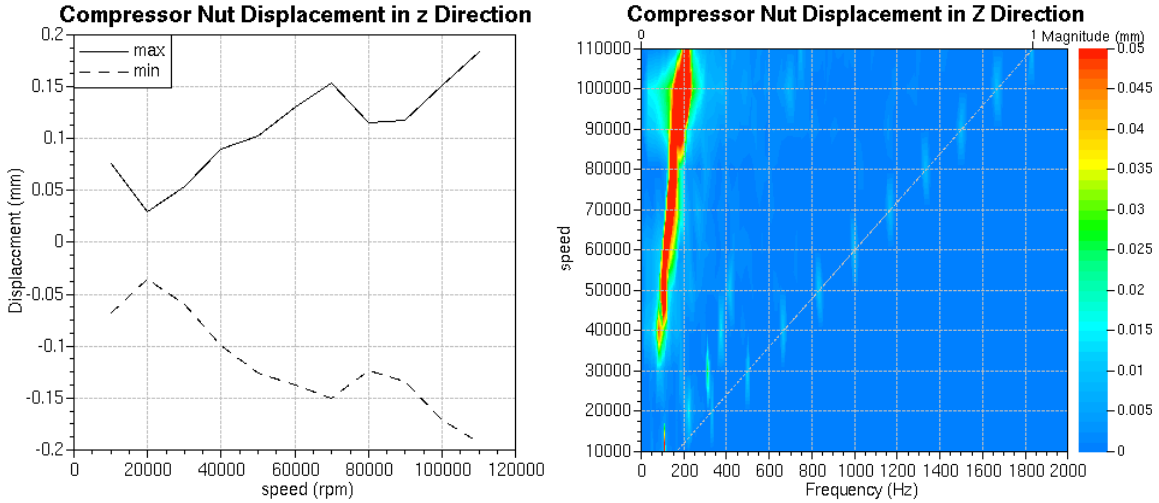

Figure 11. Maximum and minimum nut displacement in vertical direction Z for the nominal case over speed (left) and over speed (rpm) and frequency (right)

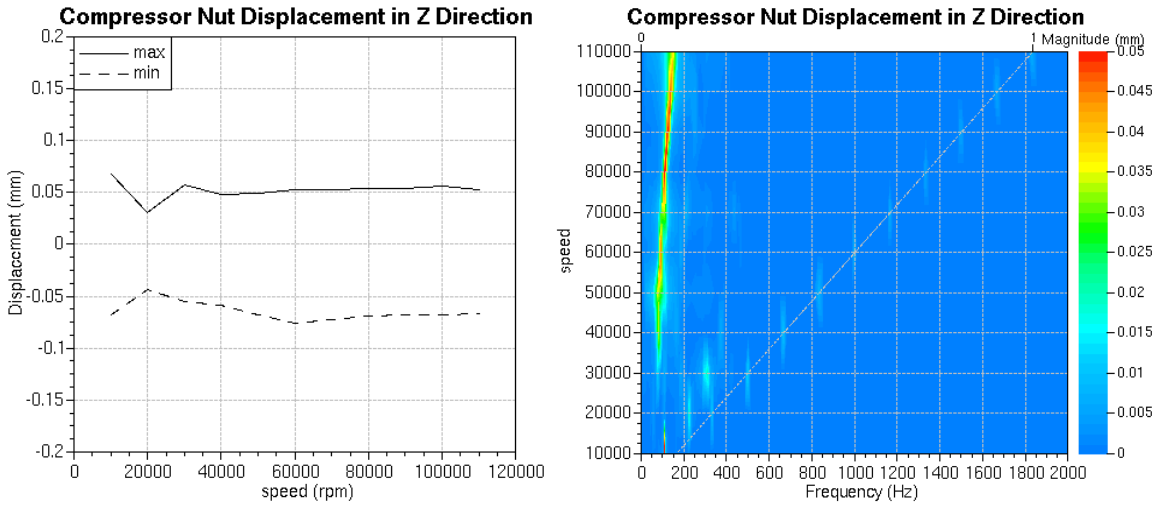

Figure 12. Maximum and minimum nut displacement in vertical direction Z for simulation with CFD and FEM pre-calculated boundary conditions over speed (left) and over speed (rpm) and frequency (right)

Similar observations can be made when looking at the orbital paths of the nut, Figure 13. Orbital paths for the nominal case and results for the case with CFD and FEM pre-calculated boundary conditions are depicted in the upper and the lower part of the figure, respectively. In case of CFD and FEM pre-calculated boundary conditions much smaller orbital paths at the nut can be observed which is influenced by smaller outer oil film clearance.

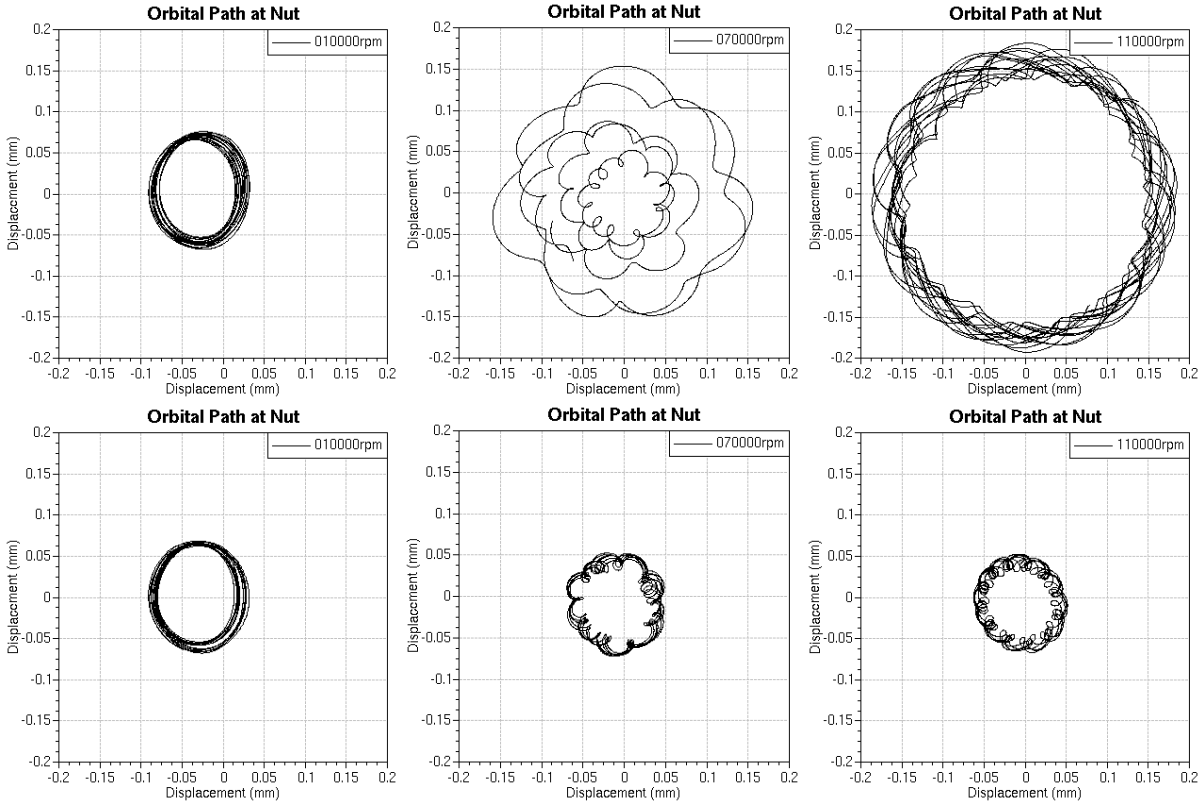

Figure 13. Orbital path at compressor nut for speed cases 10, 70 and 110 krpm: constant (top) versus variable (bottom) temperature boundary conditions

Force in the Bearings

The frequency content of the bearing forces is shown in Figure 14. The upper part of the figure depicts results for the nominal case and the lower part presents results for the case with CFD and FEM pre-calculated boundary conditions. It can be seen that the frequency content is similar for both cases. The large vibration amplitudes,

which can be observed for the compressor nut in the low frequency sub-harmonic, are also present in the bearing forces. But unlike the nut vibration, where sub-harmonic is dominant, in the bearing forces, also the first order shows large amplitudes especially at higher speeds. The bearing forces are in general smaller in amplitude, up to 100 N at outer oil film, for the case with CFD and FEM pre-calculated boundary conditions.

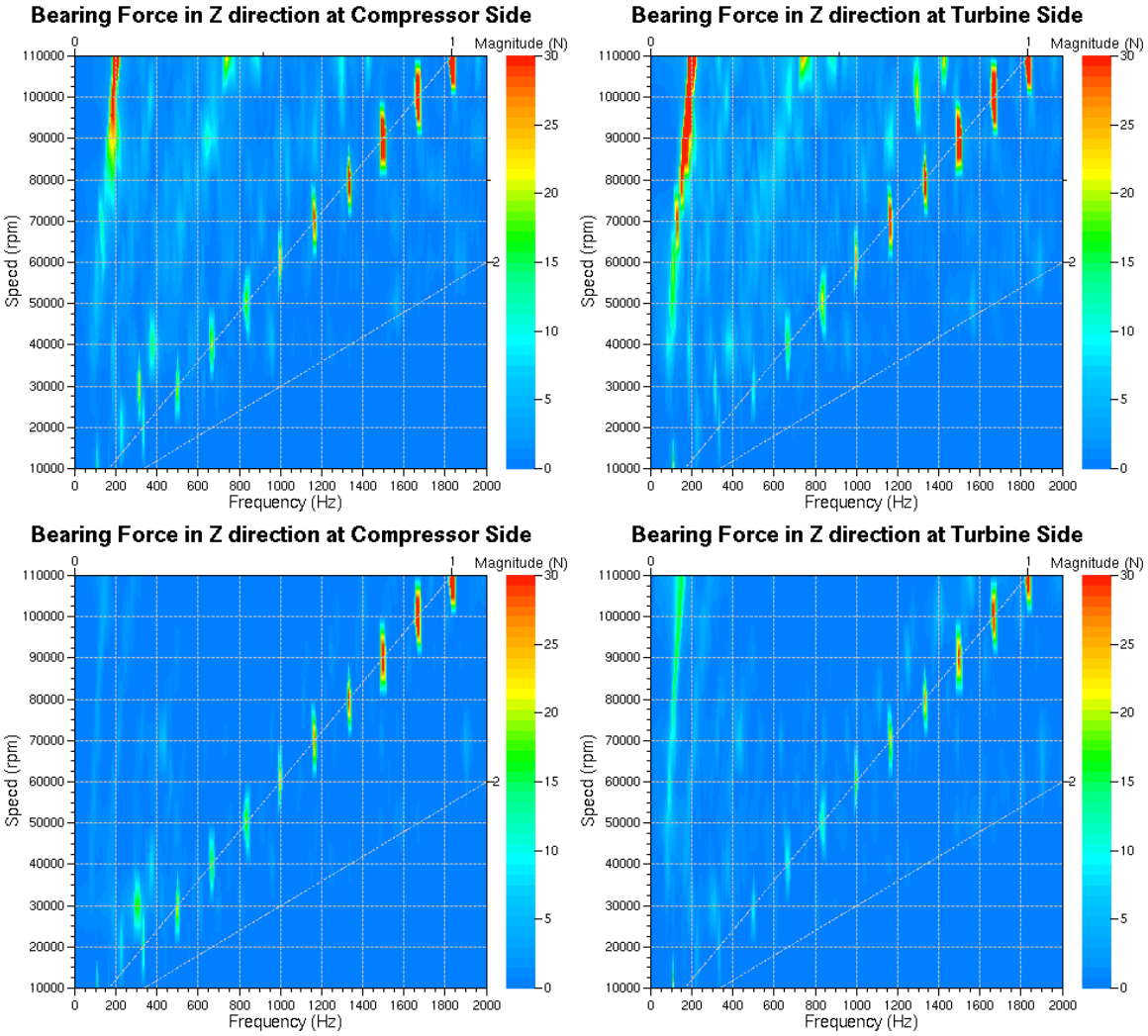

Figure 14. Bearing forces over speed and frequency for nominal case with assumed temperature (upper diagrams) versus case with CFD and FEM pre-calculated temperature (lower diagrams)

6 Conclusion

The paper shows a methodology in which it is possible to use accurately calculated oil film temperatures and according pre-calculated temperature boundary conditions for the dynamics simulation of a turbocharger. This proves to be mandatory in order to be able to compute reliable dynamic results in the complete speed range.
The paper also shows the capabilities of modern simulation tools for turbocharger applications. The same method could be applied for semi-floating bushing turbocharger design.
For full floating bushing designs, where several hundred rotor rotations are necessary to obtain steady floating bushing speeds, the drawback of the approach is long calculation time per speed, which is in the range of 2 to 24 hours per speed. Alternative to the constant rotor speeds a run-up simulation using the same simulation approach can also be an option. Such a single simulation would cover the complete rotor speed range, but would last even longer. For performing investigation shown in this paper enough processor power was available to perform constant rotor speed calculations in parallel and obtain shorter simulation time then when running a single run-up calculation.

References

Basara B., v. d. Meer A. J. and Diemath A.: Numerical simulation of fluid flow and conjugate heat transfer in a matrix of surface-mounted cubes: Evaluation of different modelling approaches; Turbulence, Heat and Mass Transfer 6; K. Hanjalic, Y. Nagano and S. Jakirlic (Editors), *Begell House, Inc.*, (2009).

AVL AST, AVL FIRE™ CFD Solver Users Guide, AVL List GmbH, Graz, (2017).

Luo J. Y., Issa R. I., Gosman A. D.: Prediction of impeller induced flows in mixing vessels using multiple frames of reference, *I. Chem. E. Symposium Series*, 136, (1994), 549–556.

Offner G.: Friction Power Loss Simulation of Internal Combustion Engines Considering Mixed Lubricated Radial Slider, Axial Slider and Piston to Liner Contacts, *Tribology Transactions*, 56, (2013) 503–515.

Drab C. B., Engl H., Haslinger J. R., Offner G., Pfau R. U. and Zulehner W.: Dynamic simulation of crankshaft multibody systems, *Journal of Multibody System Dynamics*, vol. 22(2), (2009), 133–144.

Offner G.: Modelling of Condensed Flexible Bodies Considering Non-linear Inertia Effects resulting from Gross Motions, *Proceedings of the Institution of Mechanical Engineers (IMechE), Part K: Journal of Multi-body Dynamics*, 225(3), (2011), 204–219.

Lorenz N., Offner G. and Knaus O.: Fast thermo-elasto-hydrodynamic modelling approach for mixed lubricated journal bearings in internal combustion engines, *Proceedings of the Institution of Mechanical Engineers (IMechE), Part J: Journal of Engineering Tribology*, 229(8), (2015), 962–976.

Offner G., Diwoky F., Schweiger C., Baier W.: Coupled Oil Film Lubricated Contact Simulation for ICEs, *Proceedings of the Institution of Mechanical Engineers (IMechE)*, *Part J, Journal of Engineering Tribology*, 227(5), (2013), 447–458.

Parikyan T., Resch T., Priebsch H. H.: Structured Model of Crankshaft in the Simulation of Engine Dynamics with AVL EXCITE ™, *Proceedings of the ASME 2001 Fall Technical Conference*, 2001–ICE–435, ICE 37-3, Chicago, September 23rd–26th, (2001).

Greenwood J. A., Tripp J. H.: The Contact of Two Nominally Flat Rough Surfaces, *Proceedings of the Institution of Mechanical Engineers (IMechE), Journal of Mechanical Engineering Science*, (1970-1971).

Patir N., Cheng H. S.: An average flow model for determining effects of three dimensional roughness on partial hydrodynamic lubrication, *Journal of Lubrication Technology*, 100(1), 12–17, (1978).

Address:
Advanced Simulation Technology, AVL List GmbH,
Hans-List-Platz 1, 8020, Graz, Austria
Saša Bukovnik, sasa.bukovnik@avl.com
Günter Offner, guenter.offner@avl.com
Andreas Diemath, andreas.diemath@avl.com

Department of Mechanics, University of West Bohemia,
Technicka 8, 306 14 Pilsen, Czech Republic
Luboš Smolik carlist@ntis.zcu.cz